We are IntechOpen, the world's leading publisher of Open Access books Built by scientists, for scientists

6,900
Open access books available

185,000
International authors and editors

200M
Downloads

Our authors are among the

154
Countries delivered to

TOP 1%
most cited scientists

12.2%
Contributors from top 500 universities



WEB OF SCIENCE™

Selection of our books indexed in the Book Citation Index in Web of Science™ Core Collection (BKCI)

Interested in publishing with us?
Contact book.department@intechopen.com

Numbers displayed above are based on latest data collected.
For more information visit www.intechopen.com



Chapter

Zeolites: An Emerging Material for Gas Storage and Separation Applications

Nandini Das and Jugal Kishore Das

Abstract

Zeolites are one of the amazing materials available in nature because of their structural pores. Interestingly, these god-gifted properties of zeolite can be used in gas separation and storage application. Actually, hydrogen separation and its storage are now a thrust research area. Hydrogen is considered as a 'clean energy,' which is indispensable for global affluence and alternative energy for future. But hydrogen is not accessible in its pure form during the industrial synthesis process and comes out with some other impurities like CO_2 (GHG) and other gases. So, the production of carbon-free hydrogen and its storage is so much vital. In conventional technologies, few concerns are always existed during gas separation and also in storage process. Recently, membrane-based separation process is a highly demanding technology in the industry and shows some advantages as compared to conventional process. Based on this concept, in this chapter, three different types of zeolites, that is, DDR, SAPO 34, and Bikitaite are highlighted. Here, we described the advanced synthesis process and the mechanism towards the development of high-quality nearly defect-free membranes on cheaper support. Finally, the evaluation of membranes is described through gas permeation and selectivity results of different single gas and mixture gas composition. In addition, storage capacity of H_2 by zeolite/surface-modified zeolites is included in this chapter.

Keywords: zeolite membrane, gas separation, gas storage, clean energy, pollution control

1. Introduction

Gas separation and storage processes are essentially important to various aspects in human society, such as energy consumption, environmental security, and industrial production. Energy and environmental concerns are currently at the forefront of global attention. So, carbon dioxide separation is crucial to the mitigation of greenhouse effect [1–3]. Besides, separation of hydrogen and methane together with storage is indispensable for the prevalent use of clean energy. In the case of toxic gases, the separation and storage of ammonia and carbon monoxide are important for pollution control and the synthesis of industrial chemicals. The conventional gas separation technologies such as pressure swing adsorption (PSA), cryogenic distillation, etc. are very energy intensive as well as capital intensive. Also separation methods like liquid adsorbent are cost-effective. In the distillation process, the

repeated evaporating-condensing cycle of the mixture under harsh conditions is a problematical job. Also generation of liquid adsorbent is a main concern which required the heating and cooling of massive solvent medium to release adsorbed gas. Due to these negative aspects, the potential of emerging technologies based on adsorption or membrane separations is highly amiable alternative process and has been proposed as more energy-efficient technologies [4–8]. According to existing literatures, membrane-based separation technology only consumes 10% energy of that for distillation [9]. From the industrial perspective of storage and separation of different gases, adsorption-based technique is more amicable and commendable due to its superiority to other techniques like simplicity of design, easy operation, and low cost. The separation efficiency relies on internal porosity and surface properties of solid adsorbent due to their key role in gas sorption. Alternatively, molecular properties of the adsorbent such as chemical affinity or molecular size of the separated components play a vital role in the separation process. Separation and purification, meanwhile, involve the selective adsorption of particular species from gas mixtures. Also, gas storage requires elevated pressures due to volumetric capacity considerations of porous materials and the need to deliver gas at ambient pressure or above.

Nanoporous materials have attracted huge interest among the communities of materials science, chemical engineering, and chemistry due to their excellent properties such as high surface area, large pore volume, and specific surface chemistry. The term *nanoporous* refers to any material with a pore size below ~100 nm. According to the International Union of Pure and Applied Chemistry (IUPAC) guidelines, nanoporous materials encompass both the microporous (<2 nm) and mesoporous (2–50 nm) regimes. As per literature data, porous materials like zeolites, carbon, aluminophosphates, carbon nanotubes, silica gel, pillared clays, inorganic and polymeric resins, MOFs, and MOFs composites have been investigated as adsorbents. In industry some of the adsorbents are now used for different applications. In the literature, relevant reviews and monographs have discussed the syntheses process, characterizations, and the adsorption properties of these porous materials [9–14]. The importance of porous materials for different application is summarized in the literature, which can be helpful for the next-generation researcher. Among all porous material, especially in the microporous family, zeolites are the first and foremost emerging materials and attracted increasing interest because of their unique physical and chemical properties, such as high surface area, high chemical resistance, extraordinary mechanical properties, good adsorption, and catalytic properties due to specific surface chemistry [15–22]. These peculiar and amazing properties have highlighted the potential of this material in a variety of applications and particularly in the area of gas separation and storage application [23–34]. Zeolites are traditionally referred to as a family of open-framework aluminosilicate materials consisting of orderly distributed micropores in molecular dimensions. Topologically, zeolites are three-dimensional networks of corner-sharing tetrahedral TO_4 ("T" denotes tetrahedrally coordinated Si, Al, or P), and different ways of tetrahedra connection lead to a diversity of zeolite framework types based on various compositions [35]. Silica zeolites consist of four-coordinated Si bridged by oxygen atoms [36]. To date, 235 distinct zeolite framework types have been identified in natural or synthetic zeolites, each of which has been assigned a three-letter code by the International Zeolite Association (**Figure 1**) [37].

For zeolite synthesis, the well-known conventional hydrothermal method is a widely used technique. Besides the other synthesis method like sonochemical and sonochemical-assisted hydrothermal method, microwave-assisted methods are more popular and advanced synthesis process to achieve phase pure high-quality zeolites in terms of their shape, size, porosity, uniform structure, and better crystallinity [38]. Furthermore, for the synthesis of zeolite membrane on the porous support, the in-situ and ex-situ (secondary growth) hydrothermal techniques are

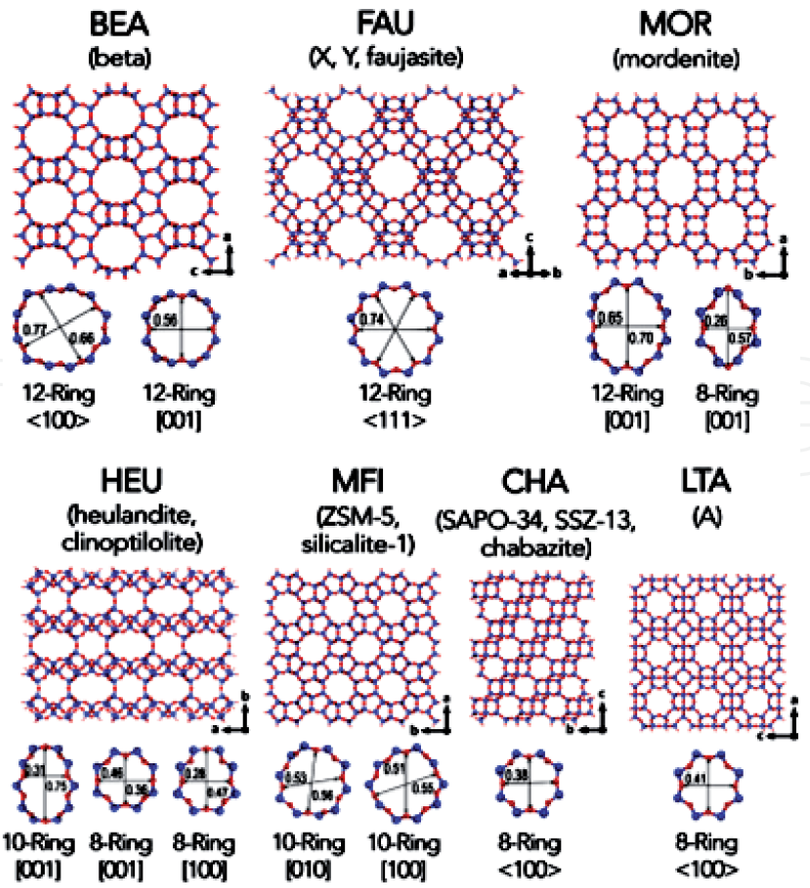


Figure 1.
Framework types of different zeolites [36, 37].

the well known process and more popular among other synthesis routes. In the case of in situ hydrothermal process, the porous support is immersed into the synthesis solution, and the membrane layer is formed directly through direct crystallization in a suitable time period. But in this process, the probability of attaining the high-quality membrane on the support is less. So ex situ hydrothermal method which is also known as seeded growth technique is an effective and accepted approach towards the development of better membrane on the support surface. This method has potential advantages in terms of achieved preferential orientation control of membrane microstructure and higher reproducibility if compared with the in situ synthesis method [39]. Extensive studies have been performed aiming at investigating potential of zeolites and derived membranes for gas separation [40–56]. Specific zeolites have a high capacity and selectivity for the gases of interest, leading to compact and efficient separation/storage systems.

To make this book chapter comprehensive, here three different types of zeolitic material were focused. The first one is siliceous deca-dodecasil 3R (DDR) zeolite which has elliptical pore openings defined by 8-member ring windows with an effective size of 0.36 × 0.44 nm^2, and it is useful for separation of small-sized gas [27, 43, 50]. Another important zeolite is silicoaluminophosphate (SAPO 34). SAPO 34, a chabazite zeolite with a composition of $Si_xAl_yP_zO_2$, where x = 0.01–0.98, y = 0.01–0.60, and z = 0.01–0.52, has an average pore size of 0.38 nm and plays an important role for gas separation application [32]. The last one is Bikitaite (BIK) zeolite having a unit cell chemical composition $Li_2(Al_2Si_4O_{12})$-$2H_2O$ [11, 36]. It is a small pore (diameter 0.28–0.37 nm) sized zeolite and has been studied for various applications and most notably has shown better performance in gas separation and storage application. The detail synthesis protocol and techniques used to synthesize zeolites and high-quality membrane have been discussed here.

After all, the performance of the developed materials was discussed elaborately for better understanding and presents the future aspect of these materials.

2. Syntheses of three different types of zeolitic material

2.1 Materials

The chemical reagents used are boehmite powder (SASOL, Germany), colloidal silica (Ludox HS- 30, Sigma Aldrich), structure directing agent (SDA) 1-adamantanamine (Sigma Aldrich), ethylene diamine (Merck, Mumbai, India), LiOH flakes (Merck, India), phosphoric acid (Qualigens fine chemicals, India), morpholine (S. D. fine chemicals, India), and deionized water.

2.2 Methods

Three unlike zeolites were synthesized by three different techniques like sonochemical, sonochemical-assisted hydrothermal method, and simple hydrothermal route. In the case of synthesis of the DDR zeolite, the sonochemical synthesis approach was implemented which is assisted by the complete growth of DDR crystal in a shorter crystallization time. The precursor solution containing the molar ratio of 1 silica:0.5 1-adamantanamine:4 ethylene diamine:100 water was used in the synthesis of the DDR crystals. The details of step-by-step synthesis process for DDR zeolite was already described in the previously reported work [40]. Two different mixtures were prepared. It is reported that first the measured amount of Ludox and water were mixed together (mixture-1). Then in another mixture (mixture-2), the ethylene diamine and water were mixed in a beaker followed by addition of 1-adamantanamine. Then the final mother sol (mixture 1 + mixture 2) was sonicated for 1 h. For fast synthesis of DDR zeolite, the ultrasound equipment (UIP1500 hd HIELSCHER Ultrasound Technology) which produces acoustic waves at frequency of 20 kHz was very useful [28]. The energy input for sonication was 250 W, and the mother sol was kept for aging for 1–9 days after sonication. The powdered products were recovered through centrifugation, washed with DI water until pH < 8, and then dried in the oven at 100°C for further characterization.

In the case of Bikitaite zeolite, the molar composition of the sol used for the synthesis was 10 Li_2O:0.5 Al_2O_3:2.5 SiO_2:600 H_2O [56]. Like the previous protocol, two reactant mixtures were prepared respectively by suspending the measured amount of colloidal silica and lithium hydroxide in deionized water (DI water) in a glass beaker (mixture 1). Mixture 2 was prepared by adding the measured amount of boehmite in lithium hydroxide. Then it was mixed slowly to mixture 1 with constant and vigorous stirring, and the mixture turned into a milky white sol. The resulting mixture was sonicated for 3 h. The energy input of sonication was varied from 150 to 250 W, followed by aging for 72 h. Then the sonicated mixture was poured into Teflon-lined stainless steel autoclave. Hydrothermal crystallization was continued under autogenous pressure in a hot air oven at 100°C for 24 h. For comparison, the different Bikitaite samples were synthesized by hydrothermal process similar to the abovementioned condition without sonication treatment. After synthesis, the zeolite powders were washed thoroughly with deionized water until the pH of the washing liquid became neutral and then dried at room temperature for further characterization.

The molar composition of the sol used for the SAPO 34 zeolite synthesis was Al_2O_3:SiO_2:P_2O_5:H_2O 1:0.3:1:66. In a typical synthesis, first boehmite powder, phosphoric acid, and the required amount of water were mixed properly by using the stirrer with 600 rpm. The mixture was stirred overnight (mixture 1).

Another mixture was prepared by dissolving the calculated amount of silica sol, morpholine, and deionized water (mixture 2). Then the reaction mixture was added slowly with mixture 1, and the resulted mother solution was stirred for another 1 hour at room temperature. The resulting mixture was stirred vigorously for 15–30 min and was kept stirring overnight to produce a homogeneous sol. The prepared homogeneous sol was kept in an autoclave, and the reaction was started at 170°C for 120 h. Finally the zeolite powders were centrifuged at 12,000 rpm for 20 min followed by washing with distilled water and the same washing process repeated four times. The resultant precipitate was dried in the oven at 100°C for 1 h.

2.3 Membrane synthesis

An indigenous clay-Al_2O_3 tube of diameter 10 mm, thickness 3 mm, and 60 mm length was used as support for synthesis of the membrane. The membranes were synthesized by secondary growth hydrothermal techniques. In this technique, first the seed layer was applied on the support by using different intermediate layer in order to attach the seed crystal and prepare a uniform seed layer on the support. Then the membranes were synthesized by secondary growth of the seed layer by hydrothermal process. The membrane synthesis procedure for SAPO 34, DDR, and Bikitaite zeolites was discussed in details in our previous work [47, 50, 56].

3. Characterization of zeolite powders and membranes

The crystalline structure of the as-synthesized zeolites and membranes was determined by XRD patterns. XRD was carried out on a Philips 1710 diffractometer using CuKα radiation (α =1.541° A). The characteristic vibration bands for zeolite powders were investigated by FTIR (Nicolet 5PC, Nicolet analytical instrument, Madison, WI). Thermogravimetric analyses (TGA) and differential thermal analyses (DTA) were performed in static air using the thermogravimetric analyzer (NETZSCH STA 409 C F3 Jupiter, Germany). The samples were heated at a rate of 10°C min^{-1} under air flow. The N_2 adsorption/desorption measurements of different zeolite powder were evaluated on a volumetric gas adsorption analyzer (autosorb-iQ-MP, Quantachrome) at 77 K. The sample used in the adsorption measurement was degassed at 423 K for 6 h before the measurements. Pore size distributions and surface area data of the synthesized powders were collected from N_2 adsorption at 77 K. The same apparatus was also used for the measurement of H_2 adsorption/desorption isotherms at 77 K up to 1 bar. Prior to adsorption study, the sample was out-gassed appropriately at 250°C for 24 h under high vacuum (106 mbar). In this case, He (99.999%) and N_2 (99.999%) were used as carrier gas. Accessible microporous volume has been estimated by using the Dubinin-Radushkevich (DR) method. Transmission electron microscopy (TEM) measurements were carried out with a Tecnai G2 30ST (FEI) operating at 300 kV. The microstructure, elemental mapping with EDAX, and cross-sectional line scanning of the synthesized membranes were examined using field emission scanning electron microscopy (FESEM: model Leo, S430i, UK). X-ray photoelectron spectroscopy (XPS) measurements of support, chemically modified support, and respective membrane were carried out on an XPS system (PHI 5000 VersaProbe II, ULVAC-PHI, INC., USA) using a monochromatic Al Kα X-ray source (1486.6 eV). To identify the bonding between seed crystal and support surface, Raman analysis was carried by Raman microscope (RENISHAW inVia, UK).

The gas permeation experiment was done by a specially designed permeation cell where the membrane was mounted in a stainless steel permeation cell and

sealed by silicone O-rings. Prior to permeation experiment, the leak test was carried out in order to obtain the correct data. The complete description of gas permeation measurement is given in the supporting information of our published paper [40].

4. Results and discussion

4.1 Formation mechanism of DDR zeolite

Siliceous deca-dodecasil 3R (DDR) zeolite has elliptical pore openings defined by 8- member ring windows with an effective size of 0.36 × 0.44 nm, and it is useful for separation of smaller-sized gas. DDR zeolites were synthesized by sonochemical method without the application of hydrothermal treatment. It is prepared only under sonication energy at different aging time ranging from 2 to 5 days. **Figure 2** shows all the characterization results of DDR zeolite obtained from XRD, IR, and FESEM. The XRD results of the sample explained the crystalline pattern, and the characteristic peaks are calculated by their (hkl) values. The acquired XRD patterns of the sample are most similar to that of the DDR structure, and the d-values are in agreement with those reported literature data [27]. The intensity and peak positions are well matched with the reported XRD patterns which explained the crystalline nature of the nanosized DDR zeolite. In the XRD pattern of sample aging for 2 and 3 days as shown in **Figure 2(a)**, the intensity increased gradually, and it confirms the more crystalline nature of the synthesized DDR zeolite (aging sample for 3 days).

Figure 2(b) shows the IR result of DDR crystals, and the strong vibration was noticed at 1377, 883, 767, 647, and 437 cm^{-1}. The characteristic band at 437 and 767 cm^{-1} was assigned to O–T–O (T = Si) bending and Si–O tetrahedral vibration, respectively. Here, more importantly the appearance of the peaks at 647 cm^{-1} was attributed to the double ring external linkage. The peaks at about 2915 and 2860 cm^{-1} correspond to the stretching vibration of 1-adamantanamine [44]. The symmetric stretching vibration of internal tetrahedron was shown at 747 cm^{-1}. **Figure 2(c)** shows the FESEM image of DDR zeolite, and elemental analysis showed that the desired atomic ratio of the DDR zeolite was obtained after 5 days of synthesis. The FESEM micrograph showed that the synthesized DDR seeds are nanosized powder having size 20 nm. The surface area of the synthesized powder was 212 $m^2 g^{-1}$. In sonochemical reaction process, free radicals are formed due to evolution of huge energy during collapsing of bubbles. It activates the reaction species which assisted in the nucleation and growth of colloidal nanoparticles of the reaction products [45]. In conventional synthesis process, the time required for complete reaction process is more which is often several days. But in sonochemical process, it needs less time for complete reaction process. From the XRD results, it can be assumed that the effect of

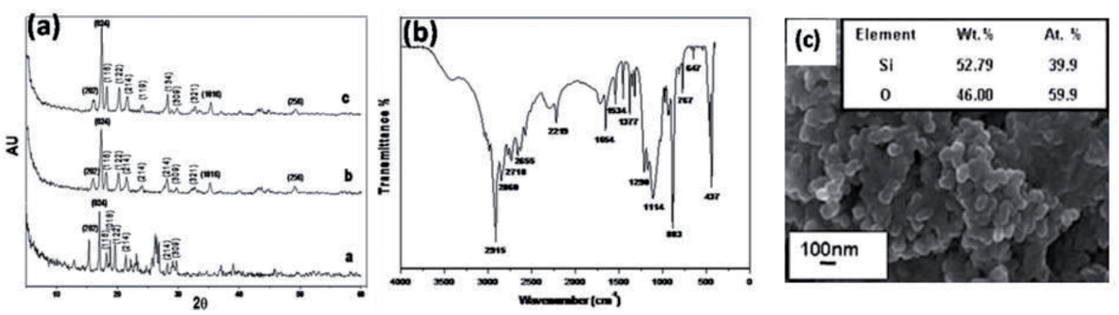


Figure 2.
(a) XRD patterns of DDR seed crystals synthesized for 2 days (lower), 3 days (middle), and 5 days (top); (b) IR spectrum of DDR zeolite synthesized for 5 days; and (c) corresponding FESEM image [43, 50].

sonication reduced the reaction time and formed crystalline DDR zeolite. The shortened reaction time is attributed to an extremely high temperature at the interface between a collapsing bubbles and the bulk solution [45]. The mass transport as well as hydrolysis and condensation reaction which were responsible for zeolite formation is controlled in this whole process. For detail, reaction mechanism and explanation in favor of this result were discussed elaborately in our reported work [42].

To develop a continuous zeolite membrane on the support surface, at first the coverage of the seed particles must be high. Generally, polycrystalline zeolite membrane contains defects (non-zeolitic pores) which are larger than zeolitic pores. The formation of non-zeolitic pores resulted from cracks and defects of the membrane layer. The non-zeolitic pores are mainly responsible for decreasing the selectivity. So in order to form a better membrane, initially seed layer plays a major role, and the adherence with the support layer is pretty much important. The lack of proper adherence of seed crystals with support may initiate the crack formation in the membrane layer. For this, different types of polymeric coating layer were used as intermediate linker between seed layer and support. The reason behind the selection of different intermediate layer and the detail mechanism were described in the literature [40, 46, 47, 50]. In the case of DDR zeolite membrane synthesis, the polymer polydiallyldimethylammonium chloride (PDADMAC) was used as intermediate linker.

PDADMAC is a high charge density homopolymer, and it can interact with several solid materials having negative surface charges. As an effect, the PDADMAC adsorbs on the alumina support primarily via electrostatic attraction between the negatively charged clay-Al_2O_3 support and the positively charged PDADMAC. Also the PDADMAC polymer can bind the negatively charged DDR zeolite particles by electrostatic attraction. As per the binding mechanism, it is assumed that due to electrostatic interaction, the negatively charged DDR zeolite particles were formed homogeneously and easily deposited on the modified support surface. This may facilitate the formation of a uniform and dense zeolite DDR membrane on the support surface. **Figure 3** shows the schematic outlook of the binding mechanism of zeolite seed layer on the support surface via using PDADMAC as intermediate linker.

The surface morphology and cross-sectional view of the synthesized DDR zeolite membrane are shown in **Figure 4(a)** and **(b)**. From the images, it can be assumed that a well-crystalline highly interlocked membrane layer was formed on the support having a uniform thickness of about 20–25 μm. Also, the phase purity of the DDR zeolite was confirmed from EDAX analysis (inset of **Figure 4(a)**), and it shows the atomic ratio of the Si and O is 1:2 which is desirable for DDR formation. The corresponding line scanning view (**Figure 4(c)** and **(d)**) throughout the membrane layer and support surface explained that the uniform membrane layer is formed on the support surface only and there is no penetration of zeolite layer into the support surface. For this outcome, intermediate PDADMAC plays a vital role. Regarding the development of continuous membrane formed or not on the support

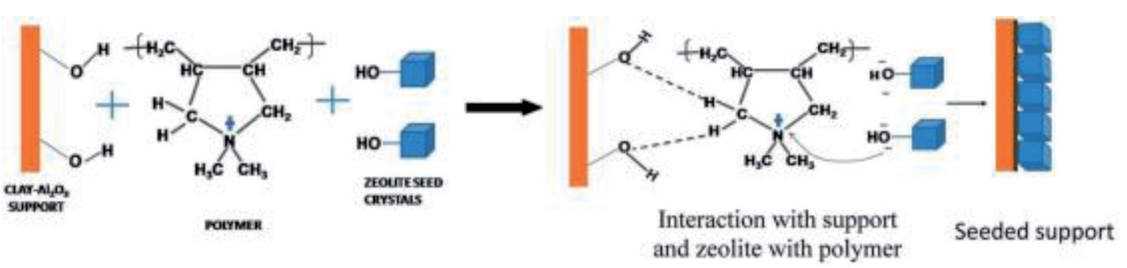


Figure 3.
Schematic of the binding mechanism between zeolite seed crystals and the support surface via PDADMAC polymer as an intermediate linker [50].

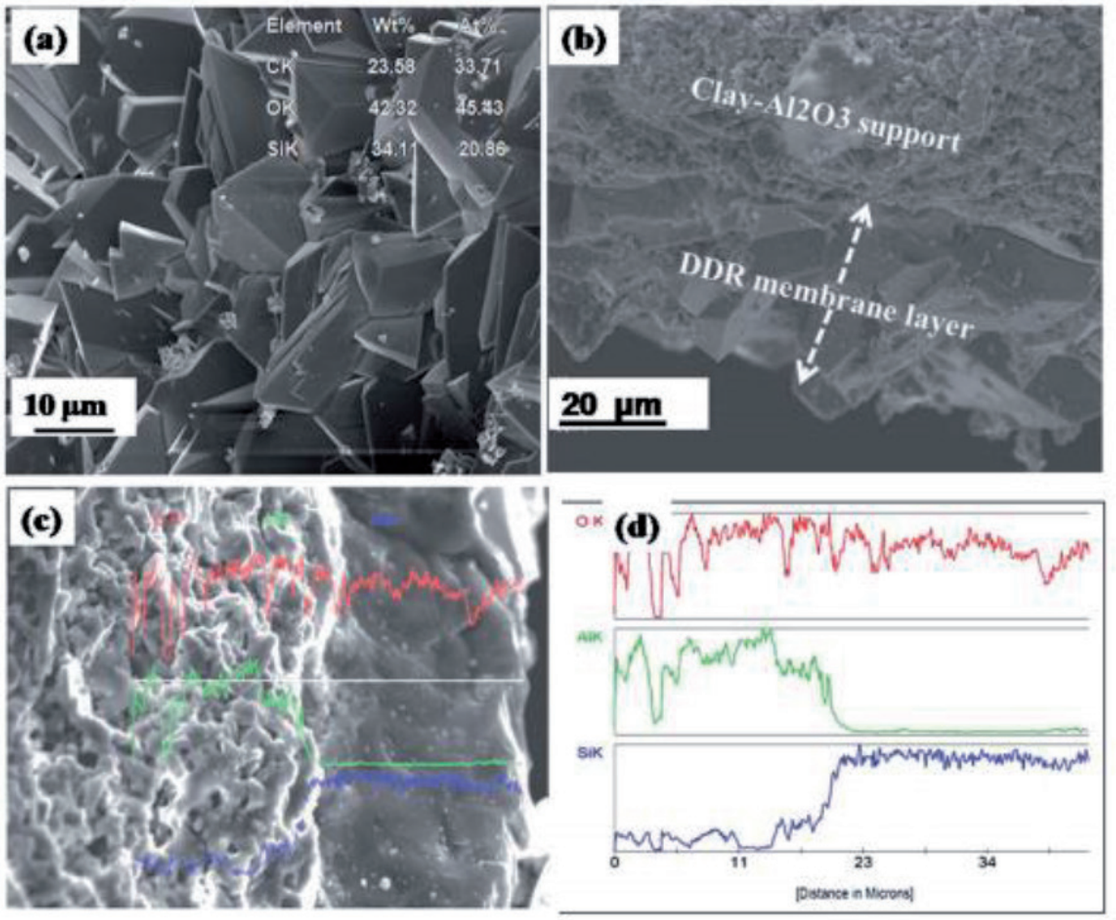


Figure 4.
FESEM images of (a) DDR membrane on the PDADMAC-modified support with EDAX data (as inset), (b) cross-sectional view of DDR membrane layer indicating the thickness by the arrow, (c) line scanning through the support and membrane layer with compositional element scan, and (d) the corresponding spectra of O, Al, and Si (distance in micron) [50].

was indicated by FESEM and XRD results. But the actual quality of the zeolite membrane can only be evaluated by gas permeation properties of the membrane.

4.2 Formation mechanism of SAPO 34 zeolite

In the case of SAPO 34 zeolite membrane, a number of studies and effort have been carried out to develop a high-quality defect-free membrane. In the literature a lot of work has been done on SAPO 34 zeolite for gas separation and storage application [32–34]. In our work an effort has been given to improvise the membrane structure and minimize the defects by different techniques for targeting the higher separation efficiency. SAPO 34 is a small pore zeolite (pore diameter of 0.38 nm), and it has a chabazite (CHA) type framework which is a promising member of the zeolite family. This interesting and efficient material has been studied for various applications. But notably its performance towards hydrogen separation from other light gases like CO_2, N_2, CH_4, etc. is quite well known [32, 33]. In the first step and prior to membrane fabrication, SAPO 34 zeolite seed crystals were synthesized by hydrothermal technique, and characterization was done systematically to know the growth of SAPO 34 zeolite during hydrothermal process. The detailed studies on the gradual formation of SAPO 34 seed crystals at different times ranging from the initial gel mixture to 120 h at 170°C were described in our previous work [51]. The XRD pattern of the zeolite powders synthesized for 120 h is shown in **Figure 5(a)**. The complete crystallization of SAPO 34 was noticed only after 120 h

of hydrothermal synthesis at 170°C. All diffraction peaks are mostly similar to those of the chabazite structure of SAPO 34, and the d-values, i.e., (100), (110), (210), (220), (211), and (131), are in agreement with those reported in the literature [32]. **Figure 5(b)** shows the FESEM image of SAPO 34 seed crystals and almost all the crystals are cubical in nature having size 2-3 micron.

The TEM image of SAPO 34 powder after 120 h of hydrothermal synthesis is shown in **Figure 5(c)**, which looks like a cubic structure, and corresponding SAED pattern reflected the CHA structure of SAPO 34 zeolite as shown in **Figure 5(d)**. **Figure 5(e)** describes the FTIR spectra of the SAPO 34 zeolite powders collected at different time starting from 0 (initial gel) to 120 h, during seed synthesis by hydrothermal method. The various zeolitic vibration frequencies were assigned in accordance to the reported literature [1]. From this study, it was confirmed that after 120 h, the complete chabazite structure of SAPO 34 zeolite is formed. The characteristic band at 480, 534, and 568 cm^{-1} was attributed to the vibration of SiO_4, (Si, Al) O_4, and PO_4, respectively. In addition, the vibration peak at 638 cm^{-1} matched with the double-6 rings (D6) would be the key evidence to CHA framework completeness. The gradual formation of SAPO 34 results at different time period, and the detail characterization was explained properly in the literature [51]. In the case of membrane synthesis, SAPO 34 zeolite membranes were synthesized on the clay-Al_2O_3 support by ex situ (secondary growth) hydrothermal method. In our approach we have prepared SAPO 34 zeolite membrane which is composed of three parts: the substrate, the intermediate layer, and the seed layer.

The intermediate layer is composed of the polymeric/inorganic oxide layer with dispersed zeolite seed crystals. The importance of intermediate layer used

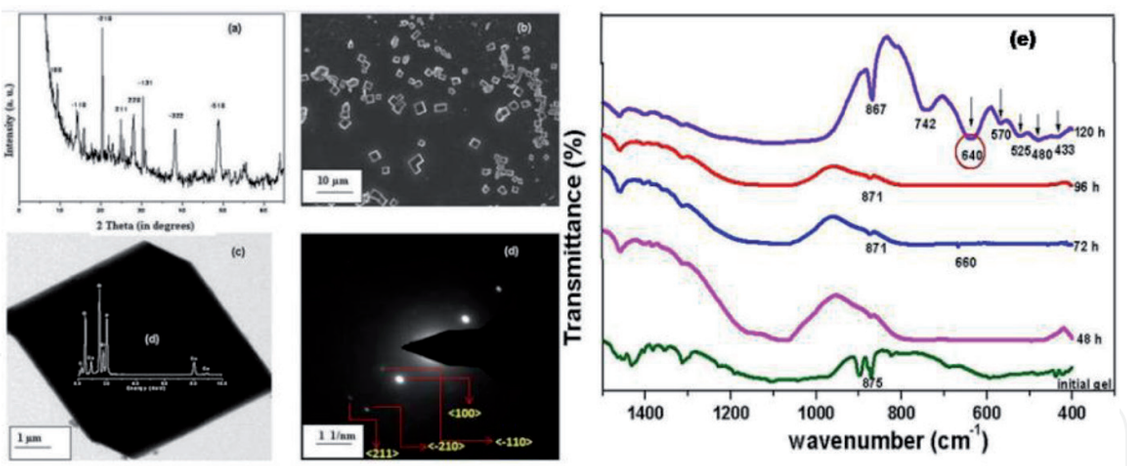


Figure 5.
(a) XRD pattern of SAPO 34 zeolite synthesized by hydrothermal technique at 170°C for 120 h, (b) FESEM image of SAPO 34 zeolite, (c) bright field TEM image synthesized powder and inset show the EDS results, (d) corresponding SAED pattern of SAPO 34 zeolite, and (e) FTIR spectra of SAPO 34 zeolite samples synthesized at different time, ranging from 0 (initial gel mixture) to 120 h of hydrothermal synthesis [46, 51].

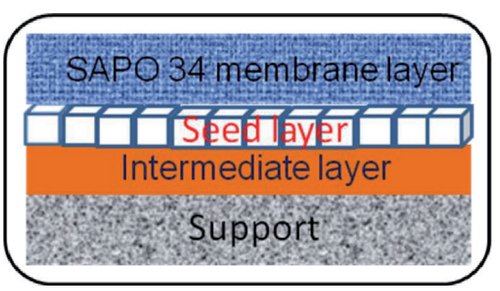


Figure 6.
Schematic representation of the different steps involved in SAPO 34 membrane syntheses.

for membrane synthesis was discussed in our reported results [40, 46, 47, 50]. The schematic representation for SAPO 34 membrane preparation is given here for better understanding (**Figure 6**).

In SAPO 34 membrane synthesis, silica intermediate layer was proposed for the selective deposition of oriented zeolite seed crystals with closely packed monolayers on a low-cost clay-Al_2O_3 tubular support and then subjected to the secondary growth under suitable hydrothermal conditions. As a result, a homogenous and reduced defect in highly oriented membrane can be synthesized simply. The organization of zeolite microcrystals with controlled orientation on substrates has been a subject of scientific interest, and recently, several approaches have been developed to prepare zeolite films with controlled orientation [52–55].

Significantly, using silica intermediate layer is predominantly based on the thermal and mechanical stability, as well as it being able to withstand in very high pressures. The silica surface under normal conditions is recovered with reactive hydroxyl groups, Si–OH, called silanol groups, and the high density of such surface –OH groups may promote high coverage of the resulting zeolite film and the highly oriented crystals. Furthermore, the implication of a silica layer plays an important role during membrane development. First of all, the layer helps to make the support surface smoother for the deposition of seed crystals in a uniform direction, and most importantly it acts as a blockade layer for the penetration of zeolite seed crystals into the interior of the support. Also it facilitates to persist the support layer with more hydroxyl (–OH) groups and as a result imparts the support with more nucleation points where crystals could bind on the support via van der Waals interactions and H-bonding [55]. In addition, it reduced stress-induced crack formation at the support–zeolite interface during calcination step [52]. The synthesized membranes were characterized by XRD, FESEM, and FESEM elemental mapping, etc. Finally the actual quality of the membrane was evaluated by gas permeation studies.

The formation of phase pure SAPO 34 membranes with a high degree of crystallinity and correct orientation was confirmed by XRD analysis. **Figure 7(a)–(d)** shows the XRD patterns of the modified and nonmodified substrate, along with the membrane layer on that substrate. SAPO 34 membrane layer prepared on the

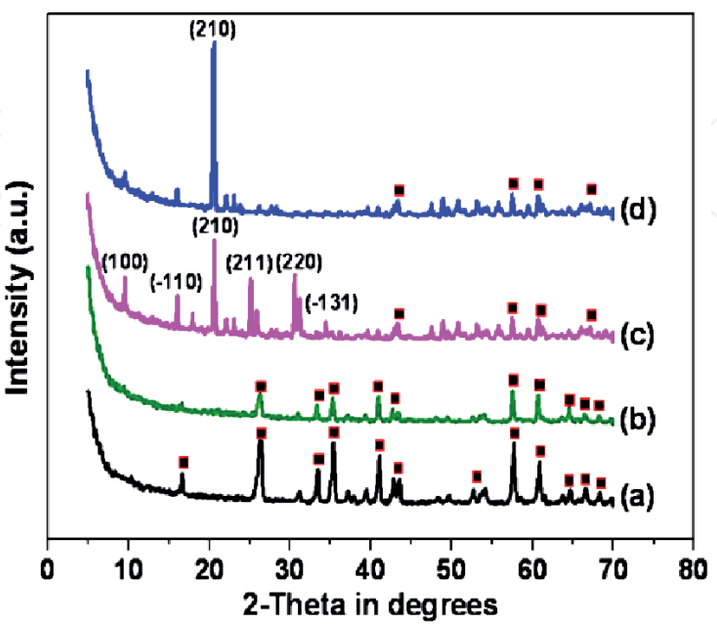


Figure 7.
XRD patterns of (a) bare support, (b) silica-modified support, (c) SAPO 34 membrane on the nonmodified support, and (d) membrane on the silica-modified support synthesized at 175°C for 120 h by hydrothermal process. (■) peak from the clay-Al_2O_3 support [40].

nonmodified support shows that all diffraction peaks are most similar to those of the chabazite structure of SAPO 34, and the intensity of the peaks like (220), (211), (131), etc. are very much prominent which indicates the presence of pure SAPO 34 crystals from the membrane surface with random orientation.

In the case of XRD pattern of the SAPO 34 membrane prepared on the silica-modified support, a quite interesting result was perceived, that is, the intensity of the (210) peak which increases drastically compared with other peaks. It can be explained that the membrane developed towards higher orientation. In addition, the membrane layer also associates with small amount of non-oriented crystals [53]. The stronger intensity of the single peak proves the possibility of formation of an oriented membrane on the silica-modified support surface which plays a vital role in determining the high performance of the membrane. The same interpretation was noticed from the FESEM results. **Figure 8(a)** and **(b)** illustrates the FESEM micrograph of the bare support and silica-modified clay-Al_2O_3 support surface, respectively. The homogeneous oriented seed monolayer on the silica-modified support is shown in **Figure 8(c)**. From the FESEM images, it can be explained that the majority of the seed crystals are deposited with proper orientation along with some disoriented seed particles interfering during the seeding process. Then during hydrothermal synthesis at 170°C for 120 h, the seed layer grows epitaxially and formed an oriented membrane layer on the support.

Figure 8(d) depicts the surface morphology of the SAPO 34 membrane layers. It shows that the support surface was totally covered by uniform and compact

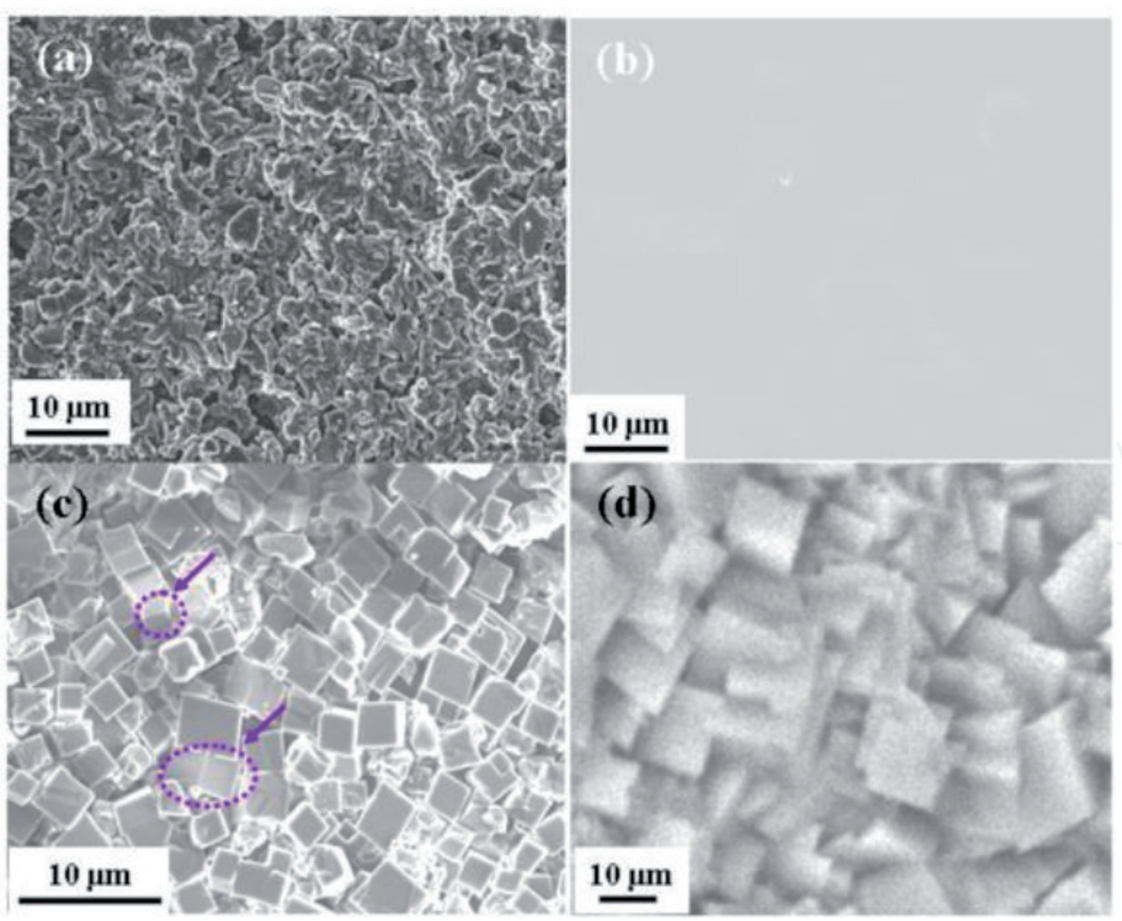


Figure 8.
FESEM micrographs of (a) clay-Al_2O_3 substrate, (b) top view image of silica-modified support, (c) oriented seed monolayer on silica-modified support with a few misoriented seeds indicated by arrow marks, and (d) oriented SAPO 34 membrane layer synthesized on the seeded support prepared at 175°C for 120 h by a hydrothermal process [40].

cubic-shaped crystals, and no visible cracks, pinholes, or other macroscopic defects were observed. The FESEM micrograph of SAPO 34 membrane layer prepared on the nonmodified support surface has already been described earlier. The comprehensible discussion was described in our published paper [46]. This work is an attempt and is anticipated to have much importance for making defect-free low-cost highly oriented membranes which could offer to be a safe, simple, and environmentally benign potential application for gas separation application. Then ultimate gas separation performance of the SAPO 34 membrane is discussed to explain the membrane efficiency.

Also another successful approach was implemented to develop an oriented defect-free membrane on the support surface. The oriented SAPO 34 membranes were grown on the support using a secondary (seeded) growth hydrothermal technique followed by insertion of 11-mercaptoundecanoic acid capped palladium (MUA-Pd) nanoparticles to the membrane.

Prior to membrane synthesis, first the clay-Al_2O_3 support was treated with polydiallyldimethylammonium chloride (PolyDADMAC) polymer, followed by deposition of seed layer homogeneously in a regular orientation on the support surface. A schematic representation of the membrane synthesis processes starting from bare support to nanoparticle insertion is shown in **Figure 9**. To deposit Pd NPs in the membrane matrix, a simple dip-coating technique was used. In practical, during thermal treatment of the Pd/SAPO 34 membrane, the instigation of defects is because of the removal of structure directing agent (SDA) from the zeolite pores. But interestingly, the presence of Pd NPs which entrapped inside the non-zeolitic pores and clogged the defects of the membrane. The synthesized membranes were characterized by XRD, TEM, XPS, and FESEM technique. FESEM and elemental mapping of the membrane cross section confirmed that most of the Pd NPs were deposited at the interface of the membrane and the support layer which may increase the membrane efficiency, i.e., separation efficiency.

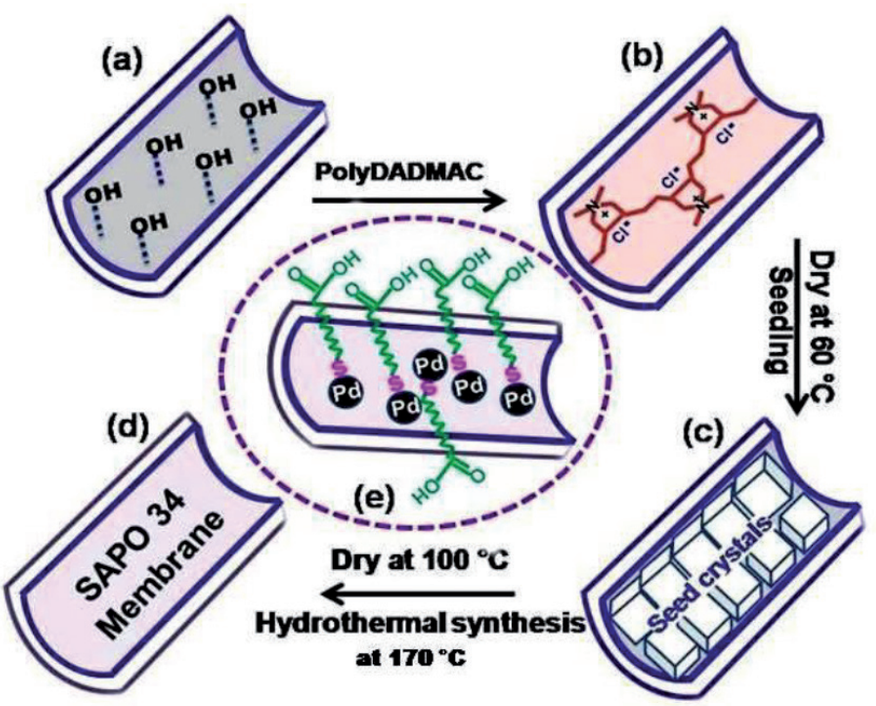


Figure 9.
Schematic representation of growth of SAPO 34 membrane starting from (a) bare substrate, (b) PolyDADMAC-modified layer to capture zeolite seed crystal, (c) seed monolayer onto the modified support, (d) synthesized membrane by secondary growth hydrothermal process, and (e) membrane layer decorated with MUA-capped Pd NPs [47].

The formation of phase pure, highly crystalline SAPO 34 zeolite on the support surface and the existence of Pd NPs on the membrane surface were confirmed by X-ray diffraction (XRD) patterns as revealed in **Figure 10**. From the XRD pattern of Pd/SAPO 34 membrane, it is clear that the intensity of the (210) peak is higher than other (100), (−110), (220), (211), and (−131) peaks and proves the presence of oriented crystals in the membrane layer. The Pd face-centered cubic phase has been identified from the Pd (111) peak which confirms the presence of Pd NPs in the membrane layer. The interpretation from the XRD results explained the presence of the Pd NPs, and the vital information is that the presence of Pd NPs did not affect the crystal structure of the SAPO 34 zeolite. It is because of the implicated nanoparticles which are too large to reside in the cavities (0.38 nm) of the framework. In general, during the heat treatment process, the structure directing agents (SDA) or any other organics are removed, and as a result, non-zeolitic pores, i.e., intercrystalline gaps, defects, or cracks, are formed.

Hence, it may be believed that the non-zeolitic pores were occupied by Pd NPs during the thermal treatment of the membrane, and further interpretation was established by FESEM studies, EDAX analysis, and elemental mapping. These results were explained in our earlier work [47]. For clear understanding, FESEM results were described here. **Figure 11(a)** depicts a FESEM micrograph of the Pd/SAPO 34 membrane layer prepared on the PolyDADMAC-modified support. It appears that a uniform membrane layer was formed with an interlocking structure. The uniformity of the membrane was achieved due to the coverage and proper orientation of seed crystals on the support which ultimately facilitated the formation of high-quality membrane. The high magnification FESEM data tells that no visible cracks, pinholes, or other macroscopic defects were noticed on the membrane layer. Then to know the membrane structure after thermal treatment, further FESEM characterization was done, and the micrograph of the calcined Pd/SAPO 34 membrane is illustrated in **Figure 11(b)**. The membrane surface was analyzed carefully by selecting different areas.

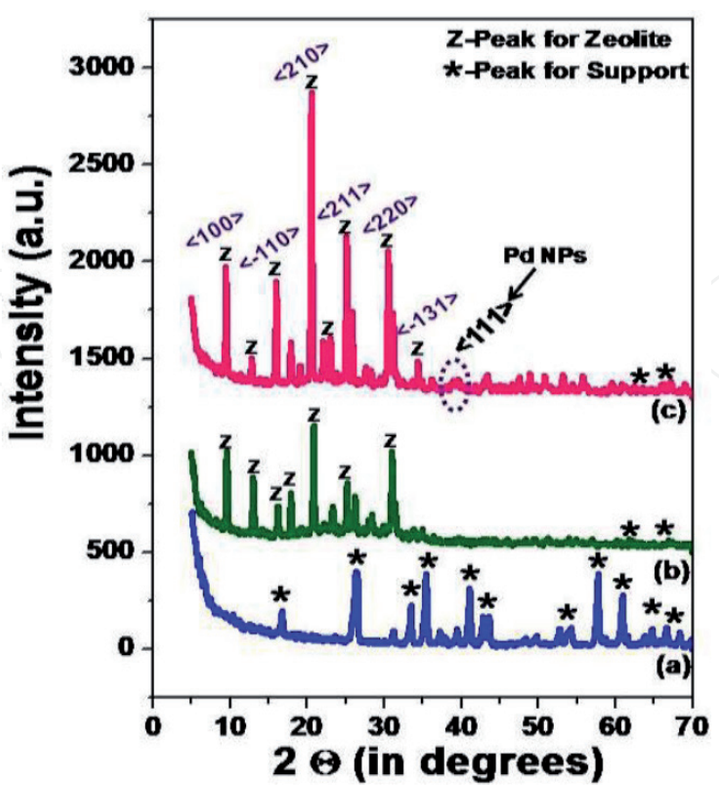


Figure 10.
XRD patterns of (a) clay-Al_2O_3 support, (b) the SAPO 34 membrane layer prepared on the nonmodified support, and (c) the Pd/SAPO 34 membrane layers on the modified support synthesized by the secondary growth hydrothermal technique [47].

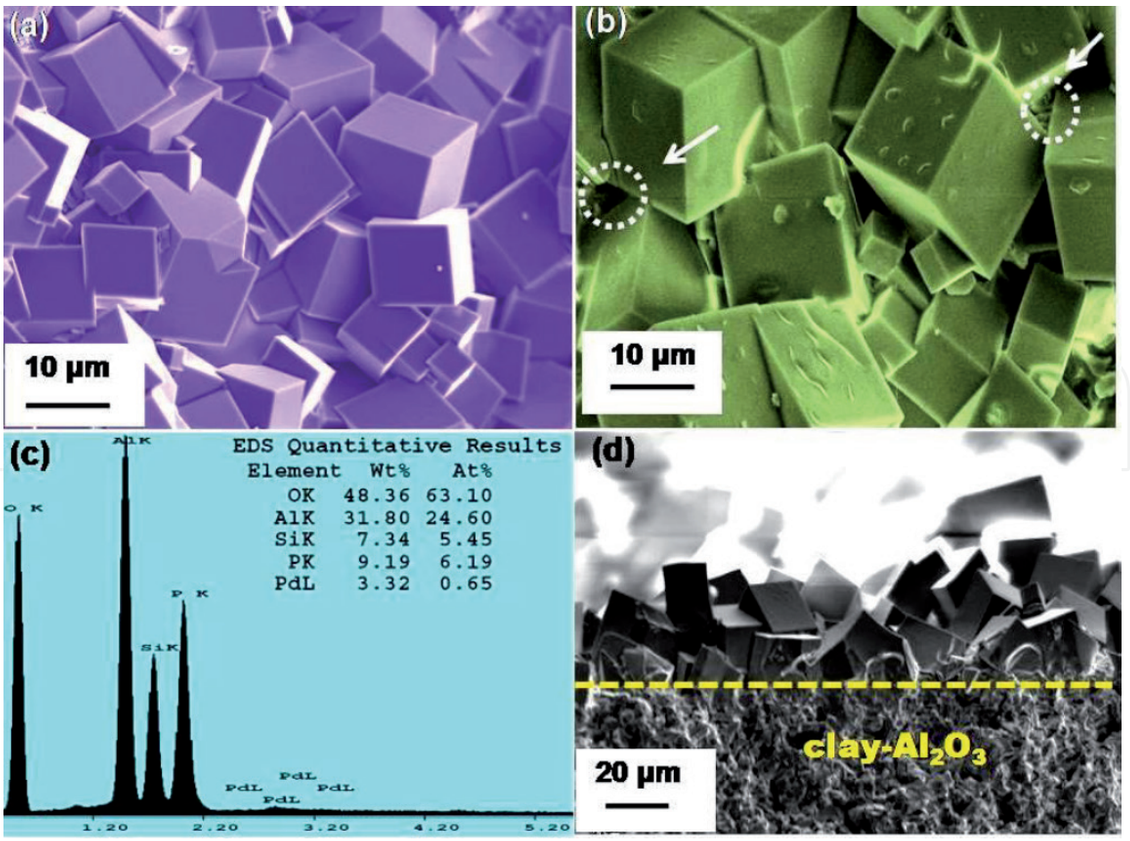


Figure 11.
FESEM micrographs of (a) Pd/SAPO 34 membrane layer, (b) calcined Pd/SAPO 34 membrane (dotted circle indicated by arrow mark shows the defects formed after calcination processes), (c) corresponding EDS spectra taken from the selected area indicated by dotted circle and the inserted table show the quantitative analysis, and (d) cross-sectional view of the Pd/SAPO 34 membrane layer [47].

During inspection, the defective areas were identified, and to verify the presence of nanoparticles inside the defective area, EDAX analysis of the same area was done (**Figure 11(c)**). The Pd peak was identified along with SAPO 34 zeolite, and Si/Al ratio confirmed the complete growth of SAPO 34 zeolite. The quantitative elemental analysis of the synthesized Pd/SAPO 34 membrane coating is described in the table inset in **Figure 11(c)**. The FESEM cross-sectional view (**Figure 11(d)**) shows that the thickness of the membrane is ~20–25 micron. The FESEM study revealed that the interlocked dense membrane was formed on the support surface successfully. However, the presence of Pd NPs which occupied and plugged into the non-zeolitic pores assisted towards the development of a nearly reduced defect membrane. It is noticed that two important phenomena were carried out simultaneously during thermal treatment. First, in the calcination process formation of non-zeolitic pores during the removal of structure directing agent, and simultaneously in the second step Pd NPs are migrating and entrapped inside the non-zeolitic pores and clogged the defects. Finally, in order to check the Pd/SAPO 34 membrane quality, gas permeation studies were carried out at room temperature in different feed pressures.

This work highlighted how the non-zeolitic pores of the synthesized membranes can be repaired by the insertion of palladium nanoparticles in the membrane matrix. Orientation and drastic reduction of non-zeolitic pores in the membrane layer may enhance the membrane quality for gas separation application.

4.3 Formation mechanism of BIK zeolite and modified BIK zeolite

Historically, activated carbons and zeolites have been the most studied microporous materials (pore diameter < 2 nm) for the storage of gases. Zeolites were the first

materials looked to as adsorbents for ANG technologies and methane adsorption in zeolites continue to assist in the understanding and design of adsorbent materials [57–58]. Zeolites as hydrogen storage materials are investigated broadly, and it is found that small molecules such as molecular hydrogen can be easily absorbed into a flexible network of zeolites, and hydrogen adsorption properties of different types of zeolites have been investigated [59–63]. It was found that the amount of hydrogen adsorbed on zeolites can be affected by the framework composition, structure, charge-compensating cations, and acidic–basic nature. In order to create strong binding sites for H_2 in zeolite pores, the importance of charge balance is quite inevitable. In this perspective, the role of light alkali metal cations such as Li^+, Na^+, and Mg^{2+} into the porous framework of zeolite plays an important role and enhances the binding energy for hydrogen adsorption [64]. Among the alkali metal cations (Li^+, Na^+, Mg^{2+}), lithium ion is more capable due to its low atomic weight and high affinity towards hydrogen by charge-induced dipole interactions [65]. Based on this concept, Li substituted Bikitaite zeolite nanocrystals are synthesized at room temperature in short crystallization time by sonochemical method. Further, ultrasonic irradiations have been used along with hydrothermal treatment for synthesis of zeolite nanocrystals. First the synthesized powders were characterized by XRD and confirmed the gradual formation of highly crystalline material. **Figure 12** shows the XRD pattern of sonochemically synthesized Bikitaite zeolite at different sonication time starting from 1.5, 2, and 3 h, and the sonication energy of 150 W was fixed for the synthesis. Before sonication, the sol was aged for 72 h at room temperature. The XRD result reveals that after 1.5 h sonication, the zeolite phase started forming and remained the same up to 3 h of irradiation. But complete growth of nanocrystalline Bikitaite phase was observed after hydrothermal treatment of sonicated sol for 24 h at 100°C. The figure clearly shows that the nanocrystalline Bikitaite zeolite with major peaks (100), (101), (201), etc. has formed and all the XRD patterns were compared with XRD pattern of simulated zeolite (COD file-969,003,103) as described in the literature [56]. Next, the morphology of the powders was observed by FESEM. **Figure 12(b)–(e)** depicts the morphology and corresponding EDAX analysis of the powders synthesized by only sonochemical method. Comparing these micrographs, it is clear that, at room temperature by ultrasonic irradiation, Li zeolite was formed with smaller size. But after further hydrothermal treatment,

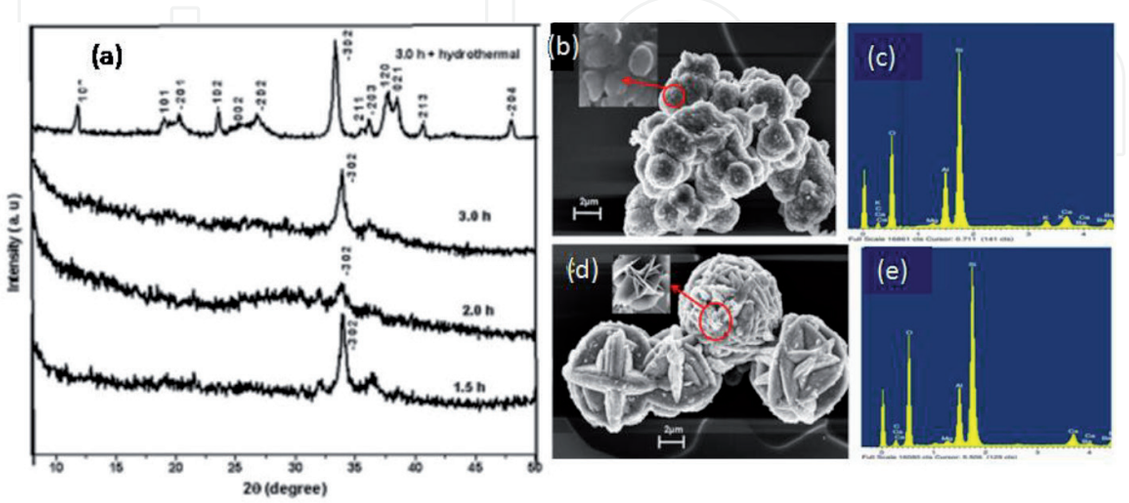


Figure 12.
(a) XRD pattern of Bikitaite zeolite synthesized with ultrasonic irradiation at different time, sonication energy of 150 W, aging time 72 h and sonication followed by hydrothermal treatment for 100°C and 24 h, FESEM micrograph of Bikitaite, prepared by (b) sonication for 3 h (inset: Higher magnified picture), (c) corresponding EDAX, (d) sonication followed by hydrothermal treatment at 100°C for 24 h (higher magnified picture is inset), and (e) corresponding EDAX [56].

primary particles formed, reflecting porous woolen ball-like structures, which finally formed flake-like flower structure (**Figure 12(d)** inset).

The EDAX result (**Figure 12(c)** and **(e)**) explained that both phases show that the presence of silica is more than alumina which is in accordance to the reported stoichiometry of Bikitaite [66].

4.4 Gas storage

Hydrogen adsorption capacity of the developed materials suited at cryogenic temperature and room temperature. The highest H_2 adsorption capacity for pure Li zeolite reached up to 1.3 wt% which is more than the reported value. The synthesized zeolite was characterized by different techniques, and then the adsorption study carried out using appropriate method. The lithium doped sample showed higher hydrogen sorption capacity showed nearly 1.3 wt% compared with other zeolite as described in literature at 77 K and 1 bar pressure. **Table 1** shows comparison of H_2 adsorption capacity of Bikitaite with other reported values of zeolite [56]. The detailed study and explanation for hydrogen storage in Bikitaite zeolite have been discussed in our recent publication [67, 68].

Finally, the study has shown that Bikitaite zeolite is a promising material for hydrogen storage. The storage volume increases with increasing Li content of the zeolite. This can be attributed by strong interaction between hydrogen molecule and high charge density of Li + ion. The detailed description of this work was reported earlier [56]. For membrane fabrication, the same powders were used as a seed for secondary growth. The mechanism and detailed procedure of membrane fabrication and their characterization results were discussed properly in the literature [69]. In this book chapter, only SAPO 34 and DDR membrane are highlighted.

Zeolite	Temperature (K)	Pressure (bar)	H_2 adsorption capacity	
			c.c/g	(wt%)
H-SAPO-34	77	0.92	122.08	1.09
H-Chabazite			123.2	1.10
(Ca-Na) Y	77.3	1.01	100	0.89
Ca-X	77.3	1.01	130	1.16
NaA	77	1.01	76.16	0.68
KA	77	1.01	11.2	0.1
CaA	77	1.01	67.2	0.6
NaX	75	1	94.08	0.84
CaA			108.64	0.97
NaA			88.48	0.79
NaX	100	60	23.52	0.21
FAU	77	1	100.8	0.9
ZSM5	77	1	80	0.71
Zeolite-L			59	0.53
MCM-41			65	0.58
Ferrierite			65	0.58
BIK	**77**	**1.01**	**143.2**	**1.3**
BIK	**298**	**1.01**	**1.0**	**0.009**

Table 1.
Comparison of H2 adsorption capacity of Bikitaite zeolite with reported values.

4.5 Gas separation

In this part gas permeation and separation studies of synthesized DDR and SAPO 34 membrane were discussed. In order to upgrade the quality of SAPO 34 zeolite membrane, different approaches have been taken as described previously. Successfully "reduced defect" or nearly "defect-free" oriented membranes were synthesized on the low-cost clay-Al_2O_3 support. The separation performances of the synthesized membrane designate whether a high-quality membrane was formed

or not. Therefore the synthesized membranes were used for gas separation studies at different feed pressures as well as different feed compositions. The separation studies were carried out at room temperature.

In the case of DDR membrane, the hydrogen separation efficiency was evaluated. Before gas permeation studies, the membranes were calcined to remove all the structure directing agents and organic compounds present in the zeolitic pore.

The permeance is expressed as the flux rate through all the pores present in the membrane. The diffusion rate becomes significantly smaller where the kinetic diameter of the gas becomes larger than the pore size of the zeolite. The molecular kinetic diameters of H_2 and CO_2 are 0.29 and 0.33 nm, respectively, which are close to the pore size of DDR zeolite. The configurational diffusion and the variation in molecular size between H_2 and CO_2 result in the difference in the rate of diffusion through the DDR zeolite channels. The diffusion rate of H_2 is faster than that of CO_2, and therefore, H_2 and CO_2 can be separated by DDR zeolite membrane. **Figure 13** describes the change of permeated flux of both H_2 and CO_2 through DDR zeolite membrane with varying transmembrane pressure difference. It shows that the rate of change of permeating flux with pressure is less for both CO_2 and H_2. In the case of molecular sieving through zeolitic pores, the rate of change of flux is pressure independent. But in this result, the little increase of flux with pressure shows that the membrane is associated with low concentration of non-zeolitic pores. At high pressure, CO_2 adsorbs more strongly than H_2 on the DDR zeolite membrane surface due to quadruple moment nature of CO_2. So rate of desorption of CO_2 from the membrane surface also decreases; as a result, permeating flux also decreases compared with hydrogen.

The real performance of the membranes can be enlightened by their mixture gas separation ability. **Figure 14** assigns the H_2/CO_2 separation factor of the mixture gas at room temperature as a function of CO_2 feed concentration at 200 kPa feed pressure for the DDR membrane. From mixture gas, it is explained that selectivity decreases with increasing CO_2 concentration. In general, CO_2 has been preferentially adsorbed on the DDR pore surface, and therefore with increasing CO_2 concentration, the extent of pore coverage has also increased. As a result, H_2 permeability decreased and selectivity reduced spontaneously. The competitive adsorption-diffusion mechanism along with molecular sieving both is playing an important role for separation process. The H_2/CO_2 separation selectivity of the membrane

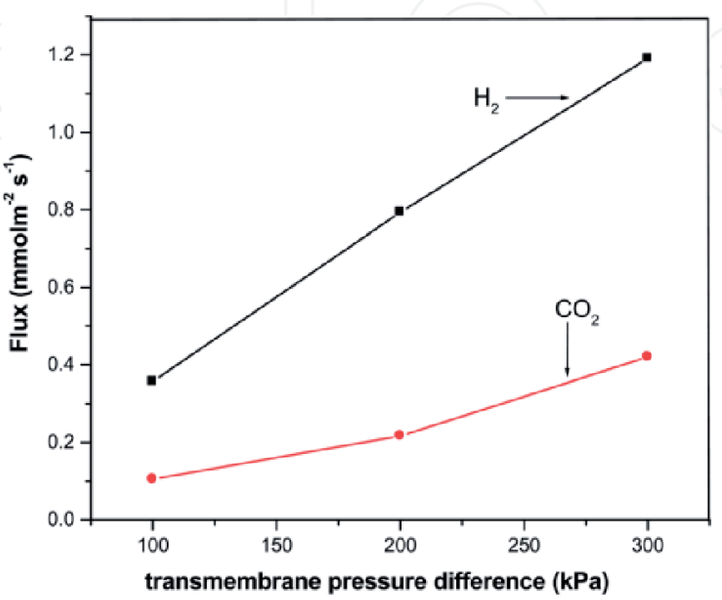


Figure 13.
Single gas permeated flux of H_2 and CO_2 as a function of transmembrane pressure difference [50].

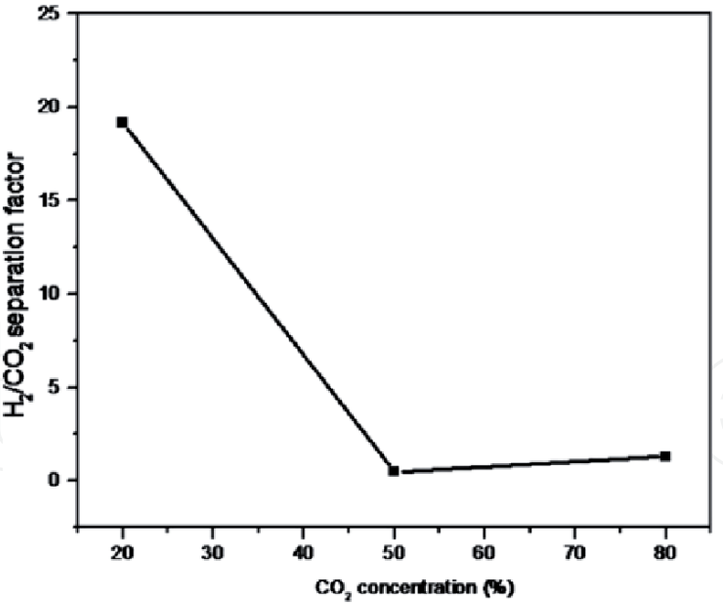


Figure 14.
H_2/CO_2 separation factor of the mixture gas at room temperature as a function of CO_2 concentration in feed at 200 kPa feed pressure for DDR membrane [50].

increased up to 3.7 at room temperature which is more than the reported values and separation mechanism explained properly in our reported work [46].

But some appreciable gas separation results were found in the case of SAPO 34 membrane synthesized on SiO_2 modified support. The SAPO 34 membrane synthesized on SiO_2 modified support shows an appreciable hydrogen separation from CO_2 and N_2. **Figure 15** shows the single gas permeation of H_2 and CO_2 at room temperature at different feed pressures. The synthesized membrane shows a relatively high hydrogen gas permeation value as compared with the literature values. Several factors might contribute to the higher hydrogen gas permeance through SAPO 34 zeolite membranes in this study. In general, the preferred orientation of the membrane layer plays a significant role in gas permeation. Generally,

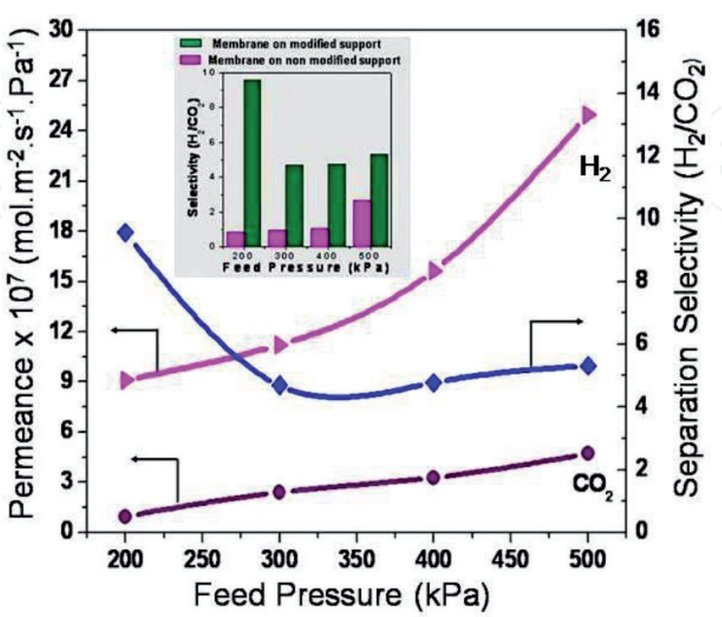


Figure 15.
Single gas permeation through SAPO 34 membrane at room temperature as a function of different feed pressures and separation selectivity of H_2/CO_2. The inset shows the comparison of separation selectivity of H_2/CO_2 by using SAPO 34 zeolite membrane prepared on the modified and nonmodified support surface [40].

oriented porous paths exhibit superior performances compared with tortuous paths of randomly oriented pores of a membrane layer by minimizing the defect density and membrane resistance.

Actually, in the case of a highly oriented membrane structure, the pores are more aligned, and the resistance of the gas transport through the aligned channel is less than that of the zigzag path of the nonaligned randomly oriented pores. As a result, membrane resistance decreases and the permeation adequacy enhanced, as compared with the randomly oriented membrane. As per our earlier discussion, the use of an intermediate silica layer which impedes the penetration of the zeolite seed particles inside the pores of the support increases the ultimate permeability of the membrane. So, combining all these aspects, it can be concluded that the almost defect-free, highly improved SAPO 34 membrane was developed on SiO_2 modified support which shows higher hydrogen gas permeance with creditable results. The configurational diffusion and the difference in molecular size between H_2 and CO_2 result in a difference in the rate of diffusion through the SAPO 34 zeolite channels. The diffusion rate of H_2 is faster than that of CO_2. The H_2/CO_2 selectivity gradually increases with respect to the different feed pressures. More interestingly, at room temperature, the appreciable highest selectivity value for H_2/CO_2 was found to be 9.12. As shown in the inset of **Figure 15**, it describes the comparative study of selectivity for H_2/CO_2, and the values were lower through the SAPO 34 membrane prepared on the nonmodified support with respect to the modified support under different feed pressures. This result indicates that there are fewer non-zeolitic pores in the case of the SAPO 34 membrane on the modified support. However, the lowest selectivity values strongly indicate the presence of non-zeolitic pores, i.e., defects in the membrane layer.

The real performance of the membranes can be investigated by their gas mixture separation ability (**Figure 16**). In the case of the H_2/CO_2 system, an appreciable selectivity value of 16.66 was obtained, and selectivity gradually decreased with increasing feed pressure. This phenomenon can be explained by the same way, i.e., an adsorption-diffusion model. At higher pressure, CO_2 adsorbs more preferentially than H_2 because it has the strongest electrostatic quadrupole moment, and more adsorption sites are generated which block some of the adsorptions of more weakly absorbing species. As CO_2 adsorbs preferentially in the SAPO 34 pore wall, it also

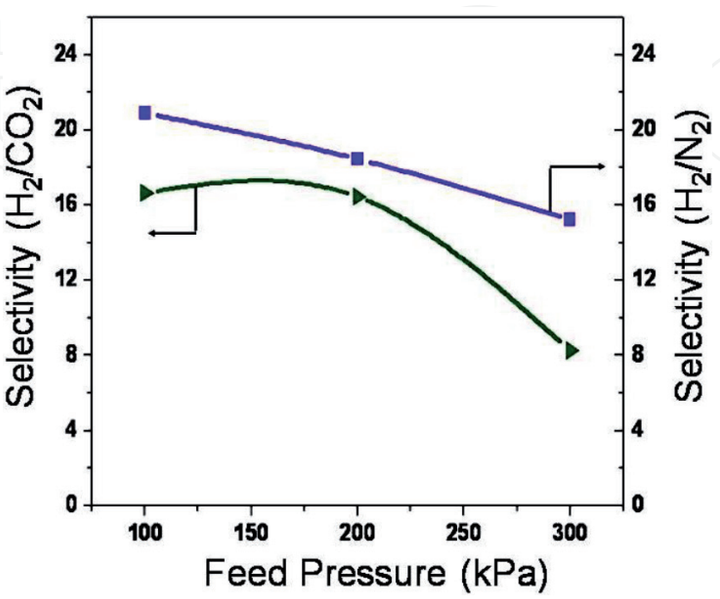


Figure 16.
Room temperature separation selectivity of 50:50 H_2/CO_2 and 50:50 H_2-N_2 mixture as a function of different feed pressures. (flow rate = 100 mL min^{-1}) [40].

desorbs and diffuses earlier than H_2, and the reasonable overall selectivity value in mixture was decreased. In H_2-N_2 gas mixture separation, a selectivity value of 20.91 was achieved and decreased to a small extent with respect to the feed pressures. Here, N_2 has a negligible effect with respect to CO_2 on H_2 during the separation process, and because of the larger size of the N_2 (0.36 nm) than CO_2 (0.36 nm), the effect of molecular sieving plays a major role in the higher selectivity. The combined effect of these two determines the ultimate selectivity of the membrane. The obtained selectivity values are improved compared with the reported literature values as described in earlier data [40]. Fascinatingly, the selectivity values were performed at high values and remain almost constant up to 80 h. The high reproducibility was due to the formation of defect-free and highly oriented membrane layers.

Next, permeation results were given here to understand the Pd/SAPO 34 membrane quality. The flow rate of different gases was controlled by the mass flow controller (MFC). **Figure 17** describes the single gas permeance of different gases through SAPO 34 membranes prepared on modified supports with and without Pd loading at 30°C and 200 kPa feed pressure as a function of the gas kinetic diameter (nm). It is interesting to note that single gas permeance through the Pd/SAPO 34 membrane at room temperature changed dramatically in comparison to the SAPO 34 membrane without Pd loading. As the kinetic diameter increased, the difference in the permeability of gases through those membranes decreased because of the difference in the kinetic diameter of gas molecule.

Mostly, the significant reduction of hydrogen permeance in the case of the Pd/SAPO 34 membrane as compared with the SAPO 34 membrane indicated the drastic reduction of non-zeolitic pores. However, in the case of the SAPO 34 membrane, the higher permeance value of H_2 was obtained because of the presence of defects. From this result, it can be concluded that the non-zeolitic pores are at a minimum in the SAPO 34 membrane after Pd NPs loading. **Figure 18** describes the change of single gas permeance of H_2 and CO_2 through the SAPO 34 and Pd/SAPO 34 zeolite membrane at different feed pressures. It can be explained that the rate of increase of the permeance values of CO_2 with feed pressure is less than that of H_2, and the explanation for this result has already been discussed. As CO_2 adsorbs preferentially on the SAPO 34 zeolite membrane surface than H_2, so the rate of desorption of CO_2 from the membrane surface also decreased as compared with H_2.

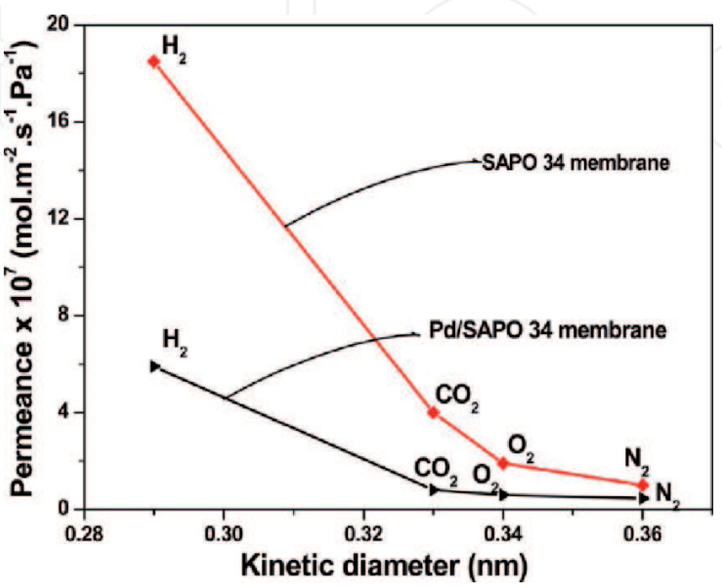


Figure 17.
Single gas permeances of different gases through SAPO 34 and Pd/SAPO 34 membranes prepared on modified supports at 30°C and 200 kPa feed pressure as a function of the gas kinetic diameter (nm) [47].

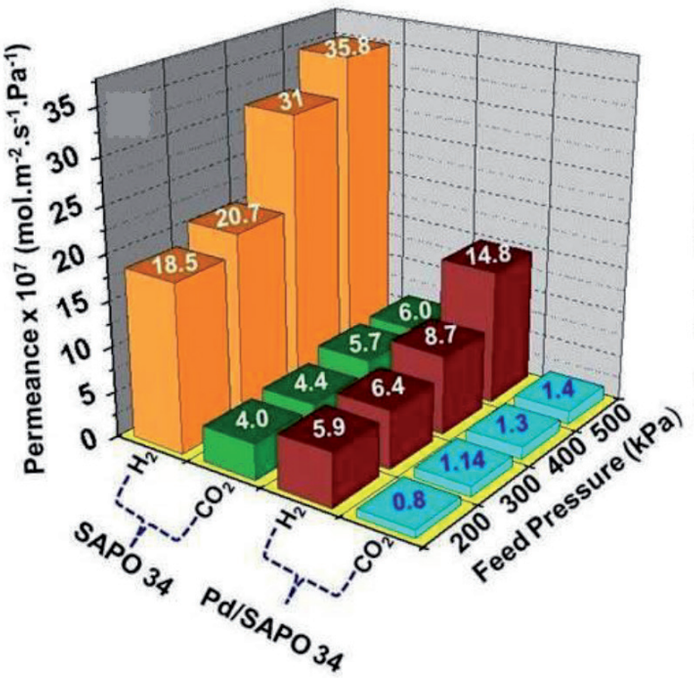


Figure 18.
Room temperature single gas permeation study of SAPO 34 and Pd/SAPO 34 membrane at different feed pressures. (flow rate 100 mL min^{-1}) [47].

Hence, due to the preferential adsorption and diffusion of CO_2 on the SAPO 34 zeolite surface and the difference in molecular size between H_2 and CO_2, there is a difference in the permeance values through the SAPO 34 zeolite channels.

According to **Figure 18**, as expected, the H_2 permeability through the Pd/SAPO 34 membrane was lower than that through the SAPO 34 zeolite membranes, and the drastic reduction of the H_2 permeance value as compared with SAPO 34 indicates that non-zeolitic pores were repaired by Pd NPs. Again, in the case of Pd/SAPO 34, the CO_2 permeance values are almost equal at different feed pressures which confirm the removal of non-zeolitic pores and permeability through the Pd/zeolite membrane mainly due to the molecular sieving process which is less dependent on feed pressure.

The real performance of the membrane for hydrogen gas separation from a mixture was evaluated from their mixture gas separation studies. The highest mixture gas separation factor for the Pd/SAPO 34 membrane was achieved at 20.8 [47]. However, the mixture separation factor in the case of the SAPO 34 membrane was 6.2. Both values, i.e., hydrogen permeation and separation factors, were higher than the literature values. Separation selectivity of the SAPO membranes increases appreciably after insertion of the Pd NPs which can reduce the non-zeolitic pores to a large extent and improve the membrane quality for hydrogen gas separation.

5. Concluding remark and outlook

We have summarized our ongoing research endeavors of microporous zeolite material for efficient gas storage and separation application. The key efforts that have been made mainly involve the synthesis of zeolite nanocrystal in a shorter crystallization time and develop the high-quality-oriented membrane on the low-cost support. To develop a high-quality membrane, different approaches have been taken and can be stated that our approach towards the development of high quality membrane is successful and may be applicable for other microporous materials for

membrane development. The detail explanation and other fundamental understanding are described in our reported paper. Also many techniques are proposed by different research groups towards the development of ideal membrane and the clear understanding can be acquired from the literature. The hydrogen storage ability of Bikitaite zeolite is really commendable, and the H_2 separation performance from H_2-CO_2 and H_2-N_2 mixture for DDR and SAPO 34 zeolite membrane is appreciable as compared with reported data. However, it should be noted that there are still many issues remaining to be addressed before implementation of industrial and commercial usage of these developed materials for separation and storage purpose. For these issues, chemists and engineering scientists of different expertise and industrial partners need to work cooperatively. In realistic separation systems, the gas mixtures and operation conditions are more complicated, and many factors need to be taken into account to perform successfully under industrial relevant condition. There is no doubt that zeolite materials are an area of great excitement and potential importance in all the areas. It would be a great achievement for such materials to be applied in practice.

Acknowledgements

The authors would like to thank CSIR, India, and also thankful to Dr. K Muraleedharan, Director, CSIR-CGCRI, for his kind permission to publish the book chapter.

Author details

Nandini Das* and Jugal Kishore Das
Ceramic Membrane Division, CSIR - Central Glass and Ceramic Research Institute, Kolkata, India

*Address all correspondence to: dasnandini@cgcri.res.in

IntechOpen

© 2020 The Author(s). Licensee IntechOpen. This chapter is distributed under the terms of the Creative Commons Attribution License (http://creativecommons.org/licenses/by/3.0), which permits unrestricted use, distribution, and reproduction in any medium, provided the original work is properly cited. CC BY

References

[1] Morris RE, Wheatley PS. Gas storage in nanoporous materials. Angewandte Chemie, International Edition. 2008;**47**:4966-4981. DOI: 10.1002/anie.200703934

[2] Jensen NK, Rufford TE, Watson G, Dongke KZ, Chan KI, May EF. Screening zeolites for gas separation applications involving methane, nitrogen, and carbon dioxide. Journal of Chemical & Engineering Data. 2012;**57**(1):106-113. DOI: 10.1021/je200817w

[3] Bae YS, Snurr RQ. Development and evaluation of porous materials for carbon dioxide separation and capture. Angewandte Chemie, International Edition. 2011;**50**:11586-11595. DOI: 10.1002/anie.201101891

[4] Li H, Wang K, Sun Y, Lollar CT, Li J, Zhou HC. Recent advances in gas storage and separation using metal-organic framework. Materials Today. 2018;**21**:108-121. DOI: 10.1016/j.mattod.2017.07.006

[5] Granite EJ, O'Brien T. Review of novel methods for carbon dioxide separation from flue and fuel gases. Fuel Processing Technology. 2005;**86**:1423-1434. DOI: 10.1016/j.fuproc.2005.01.001

[6] Ockwig NW, Nenoff TM. Membranes for hydrogen separation. Chemical Reviews. 2007;**107**(10):4078-4110. DOI: 10.1021/cr0501792

[7] Song L, Sun Z, Duan L, Gui J, McDougall GS. Adsorption and diffusion properties of hydrocarbons in zeolites. Microporous and Mesoporous Materials. 2007;**104**:115-128. DOI: 10.1016/j.micromeso.2007.01.015

[8] Adil K, Belmabkhout Y, Pillai RS, Cadiau A, Bhatt PM, Assen AH, et al. Gas/vapour separation using ultra-microporous metal–organic frameworks: Insights into the structure/separation relationship. Chemical Society Reviews. 2017;**46**:3402-3430

[9] Xu R, Pang W, Yu J, Huo Q, Chen J. Chemistry of Zeolites and Related Porous Materials: Synthesis and Structure. Asia, Singapore: John Wiley & Sons; 2007

[10] Auerbach SM, Carrado KA, Dutta PK. Handbook of Zeolite Science and Technology. New York: Marcel Dekker, Inc.; 2003

[11] Beck DW. Zeolite Molecular Sieves. New York: John Wiley & Sons; 1974

[12] Warrendale PA. Nanoporous and Nanostructured Materials for Catalysis, Sensor, and Gas Separation Applications. San Francisco: Materials Research Society; 2005

[13] Loureiro JM, Kartel MT. Combined and Hybrid Adsorbents: Fundamentals and Applications. Netherlands: Springer; 2006

[14] Schuth F, Sing KSW, Weitkamp J. Handbook of Porous Solids. New York: Wiley-VCH; 2002

[15] Srivastava R, Choi M, Ryoo R. Mesoporous materials with zeolite framework: Remarkable effect of the hierarchical structure for retardation of catalyst deactivation. Chemical Communications. 2006;**43**:4489-4491

[16] Wright PA. Microporous Framework Solids. Cambridge: RSC Publishing; 2008

[17] Corma A. From microporous to mesoporous molecular sieve materials and their use in catalysis. Chemical Reviews. 1997;**97**:23732419. DOI: 10.1021/cr960406n

[18] Corma A. State of the art and future challenges of zeolites as catalysts.

Journal of Catalysis. 2003;**216**:298-312. DOI: 10.1016/S0021-9517(02)00132-X

[19] Choi M, Cho HS, Srivastava R, Venkatesan C, Choi D-H, Ryoo R. Amphiphilic organosilane-directed synthesis of crystalline zeolite with tunable mesoporosity. Nature Materials. 2006;**5**:718-723. DOI: 10.1038/nmat1705

[20] Choi M, Na K, Kim J, Sakamoto Y, Terasaki O, Ryoo R. Stable single-unit-cell nanosheets of zeolite MFI as active and long lived catalysts. Nature. 2009;**461**:246-249. DOI: 10.1038/nature08288

[21] Kim J, Choi M, Ryoo R. Effect of mesoporosity against the deactivation of MFI zeolite catalyst during the methanol-to-hydrocarbon conversion process. Journal of Catalysis. 2010;**269**:219-228. DOI: 10.1016/j.jcat.2009.11.009

[22] Kim J, Park W, Ryoo R. Surfactant-directed zeolite nanosheets: A high-performance catalyst for gas-phase Beckmann rearrangement. ACS Catalysis. 2011;**1**:337. DOI: 10.1021/cs100160g

[23] Wu T, Wang B, Lu Z, Zhou R, Chen X. Alumina-supported AlPO-18 membranes for CO_2/CH_4 separation. Journal of Membrane Science. 2014;**471**:338-346. DOI: 10.1016/j.memsci.2014.08.035

[24] Lee I, Jeong H-K. Synthesis and gas permeation properties of highly b-oriented MFI silicalite-1 thin membranes with controlled microstructure. Microporous and Mesoporous Materials. 2011;**141**:175-183. DOI: 10.1016/j.micromeso.2010.11.012

[25] Michalkiewicz B, Koren ZC. Zeolite membranes for hydrogen production from natural gas: State of the art. Journal of Porous Materials. 2015;**22**:635-646. DOI: 10.1007/s10934-015-9936-6

[26] Das N, Kundu D, Chatterjee M. The effect of intermediate layer on synthesis and gas permeation properties of NaA zeolite membrane. Journal of Coating Technology and Research. 2010;**7**:383-390. DOI: 10.1007/s11998-009-9195-z

[27] Himeno S, Tomita T, Suzuki K, Nakayama K, Yajima K, Yoshida S. Synthesis and permeation properties of a ddr-type zeolite membrane for separation of CO_2/CH_4 gaseous mixtures. Industrial and Engineering Chemistry Research. 2007;**46**:6989-6997. DOI: 10.1021/ie061682n

[28] Li S, Zong Z, James Zhou S, Huang Y, Song Z, Feng X, et al. SAPO-34 membranes for N_2/CH_4 separation: Preparation, characterization, separation performance and economic evaluation. Journal of Membrane Science. 2015;**487**:141-151. DOI: 10.1016/j.memsci.2015.03.078

[29] Sato K, Sugimoto K, Sekine Y, Takada M, Matsukata M, Nakane T. Application of FAU-type zeolite membranes to vapor/gas separation under high pressure and high temperature up to 5 MPa and 180°C. Microporous and Mesoporous Materials. 2007;**101**:312-318. DOI: 10.1016/j.micromeso.2006.12.021

[30] Sebastián V, Kumakiri I, Bredesen R, Menéndez M. Zeolite membrane for CO_2 removal: Operating at high pressure. Journal of Membrane Science. 2007;**292**:92-97. DOI: 10.1016/j.memsci.2007.01.017

[31] Sjöberg E, Barnes S, Korelskiy D, Hedlund J. MFI membranes for separation of carbon dioxide from synthesis gas at high pressures. Journal of Membrane Science. 2015;**486**:132-137. DOI: 10.1016/j.memsci.2015.03.041

[32] Hong M, Li S, Falconer JL, Noble RD. Hydrogen purification using a SAPO-34 membrane. Journal of Membrane Science. 2008;**307**:277-283. DOI: 10.1016/j.memsci.2007.09.031

[33] Tian Y, Fan L, Wang Z, Qiu S, Zhu G. Synthesis of a SAPO-34 membrane on macroporous supports for high permeance separation of a CO_2/CH_4 mixture. Journal of Materials Chemistry. 2009;**19**:7698-7703. DOI: 10.1039/B907237C

[34] Yu M, Li S, Falconer JL, Noble RD. Reversible H_2 storage using a SAPO-34 zeolite layer. Microporous and Mesoporous Materials. 2008;**110**:579-582. DOI: 10.1016/j.micromeso.2007.06.017

[35] Li Y, Yu J. New stories of zeolite structures: Their descriptions, determinations, predictions, and evaluations. Chemical Reviews. 2014;**114**:7268-7316. DOI: 10.1021/cr500010r

[36] Baerlocher C, McCusker LB. Database of zeolite structures. Available from: http://www.iza-structure.org/databases/

[37] Li y LL, Yu J. Applications of zeolites in sustainable chemistry. Chem. 2017;**3**:928-949. DOI: 10.1016/j.chempr.2017.10.009

[38] Mintova S, Gilson JP, Valtchev V. Advances in nanosized zeolites. Nanoscale. 2013;**5**:6693-6703

[39] Bowen TC, Noble RD, Falconer JL. Fundamentals and applications of pervaporation through zeolite membranes. Journal of Membrane Science. 2004;**245**:1-33

[40] Das JK, Das N. Highly oriented improved SAPO 34 membrane on low cost support for hydrogen gas separation. Journal of Materials Chemistry A. 2013;**1**:4966-4973. DOI: 10.1039/c3ta01095c

[41] Himeno S, Tomita T, Suzuki K, Yoshida S. Characterization and selectivity for methane and carbon dioxide adsorption on the all-silica DD3R zeolite. Microporous and Mesoporous Materials. 2007;**98**:62-69. DOI: 10.1016/j.micromeso.2006.05.018

[42] Sen M, Bose A, Pal P, Das JK, Das N. Rapid synthesis of DDR zeolite at room temperature. Journal of the American Ceramic Society. 2014;**97**:52-55. DOI: 10.1111/jace.12687

[43] Zheng Z, Hall AS, Guliants VV. Synthesis, characterization and modification of DDR membranes grown on a-alumina supports. Journal of Materials Science. 2008;**43**:2499-2502. DOI: 10.1007/s10853-008-2560-y

[44] de Man AJM, Van Santen RA. The relation between zeolite framework structure and vibrational spectra. Zeolites. 1992;**12**:269-279

[45] Suslick KS, Doktycz SJ. In: Mason TJ, editor. The Effects of Ultrasound on Solids, in Advances in Sonochemistry. New York, NY: JAI Press; 1990. pp. 197-230

[46] Das JK, Das N, Bandyopadhyay S. Highly selective SAPO 34 membrane on surface modified clay-alumina tubular support for H_2/CO_2 separation. International Journal of Hydrogen Energy. 2012;**37**:10354-10364. DOI: 10.1016/j.ijhydene.2012.03.102

[47] Das JK, Das N. Mercaptoundecanoic acid capped palladium nanoparticles in a SAPO 34 membrane: A solution for enhancement of H_2/CO_2 separation efficiency. ACS Applied Materials & Interfaces. 2014;**6**:20717-20728. DOI: 10.1021/am5045345

[48] Lee JS, Kim JH, Lee YJ, Jeong NC, Yoon KB. Manual assembly of microcrystal monolayers on substrates. Angewandte Chemie, International Edition. 2007;**46**:3087-3090

[49] Yoon KB. Organization of zeolite microcrystals for production of functional materials. Accounts of

Chemical Research. 2007;**40**:29-40. DOI: 10.1021/ar000119c

[50] Bose A, Sen M, Das JK, Das N. Sonication mediated hydrothermal process – An efficient method for the rapid synthesis of DDR zeolite membranes. RSC Advances. 2014;**4**:19043-19052. DOI: 10.1039/c3ra47558a

[51] Das JK, Das N, Roy SN, Bandyopadhyay S. The growth of SAPO 34 membrane layer on support surface for gas permeation application. Ceramics International. 2012;**38**:333-340. DOI: 10.1016/j.ceramint.2011.07.011

[52] Choi J, Ghosh S, Lai Z, Tsapatsis M. Uniformly α-oriented MFI zeolite films by secondary growth. Angewandte Chemie, International Edition. 2006;**45**:1154-1158. DOI: 10.1002/anie.200503011

[53] Boudreau LC, Tsapatsis M. A highly oriented thin film of zeolite A. Chemistry of Materials. 1997;**9**:1705-1709. DOI: 10.1021/cm970151

[54] Caro J, Noack M. Zeolite membranes–recent developments and progress. Microporous and Mesoporous Materials. 2008;**115**:215-233. DOI: 10.1016/j.micromeso.2008.03.008

[55] Zhou M, Liu X, Zhang B, Zhu H. Assembly of oriented zeolite monolayers and thin films on polymeric surfaces via hydrogen bonding. Langmuir. 2008;**24**:11942-11946. DOI: 10.1021/la801879x

[56] Roy P, Das N. Ultrasonic assisted synthesis of Bikitaite zeolite: A potential material forhydrogen storage application. Ultrasonics Sonochemistry. 2017;**36**:466-473. DOI: 10.1016/j.ultsonch.2016.12.032

[57] Munson RA, Clifton RA. Natural Gas Storage with Zeolites. Washington: U.S. Dept. of the Interior; 1971

[58] Berlier K, Olivier MG, Jadot R. Adsorption of methane, ethane, and ethylene on zeolit. Journal of Chemical & Engineering Data. 1995;**40**:1206-1208. DOI: 10.1021/je00022a011

[59] Broom DP. Hydrogen Storage Materials: The Characterization of their Storage Properties. London: Springer-Verlag London; 2011. pp. 19-59

[60] Prasanth KP, Pillai RS, Bajaj HC, Jasra RV, Chung HD, Kim TH, et al. Adsorption of hydrogen in nickel and rhodium exchanged zeolite X. International Journal of Hydrogen Energy. 2008;**33**:735-745. DOI: 10.1016/j.ijhydene.2007.10.047

[61] Zhang SY, Talu O, Hayhurst DT. High-pressure adsorption of methane in zeolites NaX, MgX, CaX, SrX and BaX. The Journal of Physical Chemistry. 1991;**95**:1722-1726. DOI: 10.1021/j100157a044

[62] Cavenati S, Grande CA, Rodrigues AE. Adsorption equilibrium of methane, carbon dioxide, and nitrogen on zeolite 13X at high pressures. Journal of Chemical & Engineering Data. 2004;**49**:1095-1101. DOI: 10.1021/je0498917

[63] Nijkamp MG, Raaymakers JEMJ, van Dillen AJ, de Jong KP. Hydrogen storage using physisorption-materials demands. Applied Physics A: Materials Science & Processing. 2001;**72**:619. DOI: 10.1007/s003390100847

[64] Hassani SS, Salehirad F, Aghabozorg HR, Sobat Z. Synthesis and morphology of nanosized zeolite L. Crystal Research and Technology. 2010;**45**:183-187. DOI: 10.1002/crat.200900450

[65] Regli L, Zecchina A, Vitillo JG, Cocina D, Spoto G, Lamberti C, et al. Hydrogen storage in chabazite zeolite frameworks. Physical Chemistry

Chemical Physics. 2005;**7**:3197-3203. DOI: 10.1039/B509124A

[66] Kocman V, Gait RI, Rucklidge J. The crystal structure of bikitaite, LiAlSi2O6H2O. American Mineralogist. 1974;**59**:71-78

[67] Palomino GT, Bonelli B, Areá CO, Parra JB, Carayol MRL, Armandi M, et al. Thermodynamics of hydrogen adsorption on calcium exchanged faujasite-type zeolites. International Journal of Hydrogen Energy. 2009;**3**:4371-4378

[68] Li J, Wu E. In: Andreyev MK, Zubkov OL, editors. Storage of Hydrogen in Zeolites in Zeolites: Synthesis, Chemistry and Applications. New York: Nova Science Publishers, Inc; 2012. pp. 149-170

[69] Roy P, Das N. Synthesis of NaX zeolite-graphite amine fiber composite membrane: Role of graphite amine in membrane formation for H_2/CO_2 separation. Applied Surface Science. 2019;**480**:934-944. DOI: 10.1016/j.apsusc.2019.03.038